12,14

Experimental irradiation of polyethylene composites with neutrons and γ-quanta

© N.I. Cherkashina[1], V.I. Pavlenko[1], D.S. Romanyuk[1], R.V. Sidelnikov[1], P.I. Rudnev[2], I.V. Cheshigin[2]

[1] Belgorod State Technology University named after V.G. Shukhov,
Belgorod, Russia
[2] ADC Center,
Moscow, Russia

E-mail: romanyuk.dmitrij.98@bk.ru

Received November 18, 2024
Revised February 28, 2025
Accepted March 5, 2025

The article presents the results of a study of polymer composite materials based on high-pressure polyethylene C_nH_{2n+2}, boron carbide B_4C and titanium hydride TiH_2 for protection against the effects of neutrons and γ-quanta. The article presents a technology for manufacturing materials with the following composition: C_nH_{2n+2} — 40 % wt., B_4C — 5 % wt., TiH_2 — 55 % wt. (PCM-TiH_2-B_4C) and C_nH_{2n+2} — 95 % wt., B_4C — 5 % wt. (PCM-B_4C). The flexural strength of PCM-TiH_2-B_4C is 12.5 MPa, and that of PCM-B_4C — 4.8 MPa. The structure of the materials is considered and described using electron microscopy, and flaw detection is carried out to assess the quality of the resulting composites and remove defective samples. The interaction of ionizing radiation with materials was simulated using the XCOM 3.1 program. The neutron flux attenuation coefficient was determined experimentally: at an energy of 2 MeV for PCM-B_4C it has a value of 73.3 cm^{-1}, and for mboxPCM-B_4C-TiH_2 its value is — 128.5 cm^{-1}. The γ-quanta flux attenuation coefficient, established experimentally, was estimated: at an energy of 2.5 MeV for PCM-B_4C this coefficient has a value of 10.3 cm^{-1}, and for PCM-B_4C-TiH_2 — 19.22 cm^{-1}.

Keywords: polyethylene, titanium hydride (TiH_2), composite protective material, attenuation coefficient.

DOI: 10.61011/PSS.2025.03.60888.311

1. Introduction

Study of the ionizing radiation interaction with various media is of key importance in the design of radiation protective shields. Neutron and γ-radiation are a significant problem in such areas as nuclear power engineering, medicine and aerospace engineering [1]. Protective materials against γ-radiation and neutrons are a basic class in the nuclear engineering and radiological protection. Ionizing radiation, such as γ-quanta and neutrons, may significantly damage the nearby equipment and people due to its strong penetrating power. Long-term exposure to radiation of neutrons and γ-quanta may damage live tissues, electronic components and structural materials [2,3]. Therefore, development of effective materials for protection against neutron and γ-radiation is an important task to ensure safety and reliability in these areas. Traditional materials for the protection against γ-radiation, such as lead, have limitations due to the considerable weight of the protection and its toxicity [4–6].

Recently composite materials were used as a promising solution for protection against neutron and γ-radiation. Combining various materials with unique properties, one may achieve the improvement of the radiation protective properties of a composite material, reduce weight and improve safety [7–13].

A composite is known on the basis of polymer nanocomposites from epoxide resin and nanoparticles HfB_2 [14]. This composite material has good γ-radiation attenuation rates, but practically has no impact at neutron flux. To improve the absorption of the neutron and γ-radiation, it is necessary to create composite materials, which may handle large number of radiations, which was studied in paper [15]. In the composite material presented in paper [15] the matrix is polytetrafluorethylene (PTFE), and the filler — bismuth oxide (Bi_2O_3), tungsten carbide (WC), titanium hydride (TiH_2), boron carbide (B_4C). This composite material handles well the moderation of fast neutrons down to thermal ones, and the decrease in the intensity of neutron radiation. However, paper [15] lacks data on absorption of γ-quanta, which prevents full assessment of the material protective ability.

Besides, materials with hydrogen in their composition are also of great interest in the study of the issue of protection against neutrons due to the hydrogen's ability to moderate fast neutrons down to thermal ones [16–18]. Compared to ordinary hydrogen materials, metal hydrides, which are rich in hydrogen, maintain their properties at high temperatures and, moreover, have good mechanical properties [19–22].

Metal hydrides have a property of fully reversible hydrogen storage and good volume hydrogen capacity. Hydrogen density makes it attractive as a neutron protection. In many literature sources the potential use of metal hydrides as nuclear materials in fast neutron reactors was investigated. In the space industry the metal hydrides, such as titanium hydride and lithium hydride, may be used as radiation protection in spacecraft [23].

This paper presents the study of the composite material based on high pressure polyethylene (HPPE) with filler from titanium hydride (TiH_2) and boron carbide (B_4C). Physical and mechanical parameters of specimens were evaluated, and experimental studies were conducted to assess their radiation protective properties in respect to neutron and γ-radiation.

2. Materials and methods

2.1. Materials

To produce a composite material, the matrix was (HPPE) of grade 15303-003, (purity $> 99\,\%$, density $900-930\,kg/m^3$, melting temperature $100-115\,^\circ C$) (OOO „Kazanorgsintez“, Russia), and the filler was two compounds: 1) boron carbide (B_4C), average particle size $0.10-120\,\mu m$, $\rho = 2.52\,g/cm^3$, (OOO „Platina“, Russia) and 2) pellets of titanium hydride (TiH_2) (GOST 14-1-2159-77), (OOO „RUSKHIM“, Russia). The average pellet diameter was $\sim 0.2-2.5\,mm$. After grinding the average particle size was $0.20-150\,\mu m$.

2.2. Manufacture of composites

The composite material was manufactured in several stages. The first stage was preparation of the fillers: pellets of titanium hydride (TiH_2) were ground in a ball impact mill, with subsequent sieving through a sieve with cell size of $64\,\mu m$. Further the produced powder of titanium hydride and carbide was placed in a ball mill without addition of grinding bodies, where two components of the filler were mixed. Then the produced mix was dried in an air oven at $110\,^\circ C$, for 10 min.

The second stage was polyethylene preparation: from beads of (HPPE) using a jaw crusher (JC 6 M) powder was produced with size of $130-200\,\mu m$. HPPE powder was first dried in an air oven at $70\,^\circ C$, for 15 min, with further sieving through a sieve of $140\,\mu m$. Then the prepared material (HPPE) was loaded in a ball mill with previously prepared filler according to the ratio. After loading of the material, the grinding bodies were added at the ratio of 20 : 1 by weight. Further the materials were homogenized for 3 min. Then grinding bodies were withdrawn from the prepared material.

Stage 3: the prepared material was exposed to hot pressing in a die at specific pressure of 125 MPa, using a steel die with constant heating and soaking at $140-160\,^\circ C$ for 20 min. After die cooling, the material was withdrawn and then polished. The finished specimens had dimensions of $L = 98\,mm$, $B = 22.5 \pm 2.00\,mm$, $H = 98\,mm$.

The same method was used to prepare the specimens that contain only 5 % wt. B_4C.

2.3. Equipment and research methods

To study the structures, scanning electron microscope (SEM) Tescan MIRA (Tescan, Brno, Czech Republic) of 4th generation with Schottky cathode was used. The instrument makes it possible to make quality SEM-images of the material surfaces and test the elemental composition in real time. It has a convenient interface and simplifies data collection on the local composition of specimens.

Bend tests were carried out using test machine REM-100 (OOO „METROTEST“, Republic of Bashkortostan, Neftekamsk, Russia). The bending strength was determined using standard methods according to GOST ISO 17138:2014. Loading was carried out for the three-point bending tests.

Measurements of the energy distributions of fast neutron flux and γ-quanta were carried out with spectrometer-dosimeter SDMF-1608SN (OOO „ADC“, Moscow, Russia) [24] in the energy range of neutrons $\sim 0.8-16\,MeV$ and γ-quanta $\sim 0.1-9\,MeV$.

The source of fast neutrons and γ-quanta was a point isotropic source with energy spectrum close to fission spectrum U^{235}.

Table 1. Composite parameters

Material	Density, g/cm^3	Nuclear density, cm^{-3}	Thickness, cm
PCM-V_4C	0.9267	$1.81 \cdot 10^{23}$	15
PCM-V_4C-TiH_2	1.619	$1.198 \cdot 10^{23}$	16.29

Table 2. Mass fraction of substance in composite materials

Composite	Name	Percentage ratio, %
PCM-V_4C-TiH_2	C	35.34
	H	7.97
	B	3.91
	Ti	52.78
PCM-VB_4C	C	82.6
	H	13.5
	B	3.9

3. Results and discussion

3.1. Material specifications

For the research, the materials were produced, which contained the following components:

- HPPE (C_nH_{2n+2}) 40 % (by weight), boron carbide B_4C — 5 %, titanium hydride (TiH_2) — 55 % (material designation PCM-TiH_2-B_4C).
- HPPE (C_nH_{2n+2}) 95 % (by weight), boron carbide (B_4C) — 5 % (material designation PCM-V_4C).

Table 1 presents physical values of the studied materials necessary to calculate the full sections of interaction. Table 2 specifies the mass fraction of the substance in composite materials.

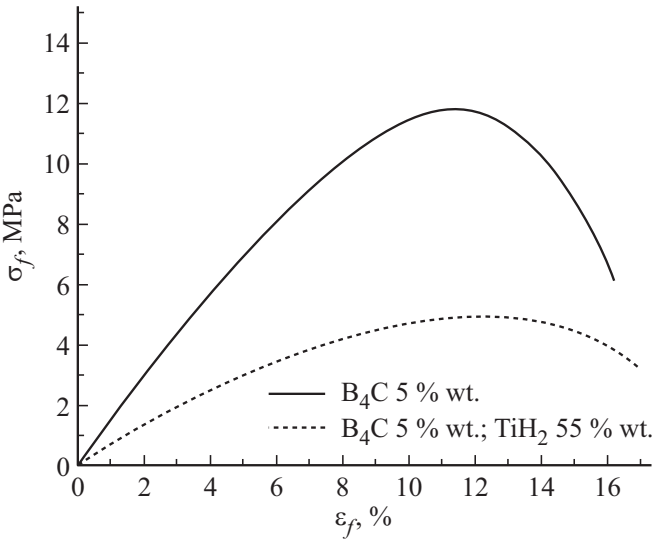

Figure 1. Schedule of dependence of applied load on specimen deformation.

3.2. Studies of strength characteristics of material

Specimens of composite materials were studied on test machine REM-100. Data of specimen three-point bending testing are provided in Figure 1.

The curve shows the results of the study of strength characteristics of composite materials which contain B_4C (boron carbide) in the amount of 5 % wt., and also additive TiH_2 (titanium hydride) in the amount of 55 % wt.. The curve reflects the dependence of limit stress (σ_f) on deformation (ε_f) in three-point bending. Composite PCM-V_4C, B_4C (5 % wt.) demonstrates high limit stress (above 12 MPa). When composite was tested PCM-V_4C-TiH_2 with boron carbide and titanium hydride content in the composition (B_4C 5 % wt. + TiH_2 55 % wt.) specimens demonstrated average value of 4.8 MPa. Both materials demonstrate plastic behavior, but the composite only from B_4C (5 % wt.) reaches higher deformation value ($\varepsilon_f \approx 14\%$), while addition of TiH_2 results in the reduction of the limit deformation. Note that compared to the specimen of borated polyethylene the composite with the content of titanium hydride (TiH_2) lost 61.60 % strength, which is related to higher % of filling. Based on the produced data, one may conclude that the composite material containing 55 % wt. TiH_2 and 5 % wt. B_4C, demonstrates satisfactory strength under three-point bending, providing for stable mechanical characteristics. Even though its limit stress is lower compared to pure B_4C (5 % wt.), the material maintains sufficient structural capacity, which makes it promising for use in the items that require balance between strength and plasticity.

Addition of TiH_2 helps to change the damage mechanism, potentially improving the energy capacity of deformation and providing for a combination of strength and deformation properties, which may be critical for engineering solutions, which require control over damage and improved impact strength.

3.3. Specimen microscopy

Using the method of scanning electron microscopy, microphotographs of composite material fracture were obtained PCM-V_4C-TiH_2 (Figure 2).

The main purpose of microscopy is visual inspection of particle size and distribution in the material. To obtain a fracture, a standard method was used for liquid nitrogen freezing of specimens applied to obtain a clear undistorted structure of the specimen, which is critical for microstructure analysis. It is especially true for brittle materials.

Figure 2, *a* clearly shows particles of fillers, which are evenly distributed in the matrix. At larger magnification of Figure 2, *b* and *c* the particles of irregular shape with rough edges become more discernible. Particle size may be defined using Figure 2, *c*. The bulk of the particles have the size of up to 20 μm. Due to various contrast in SEM-images, it is possible to identify the particles association. Since titanium (Ti) in the composition of titanium hydride has a higher atomic number, it releases more secondary electrons, which makes its areas lighter, while boron carbide absorbs more electrons and emits less secondary electrons, which makes its areas darker. Therefore, different contrast in the images is caused by the difference in the atomic structure of the materials, their interaction with the electron beam and as a result the number of the emitted secondary electrons. Discernible particles of carbide have a large structure with size of $\sim 10-20\,\mu$m.

Figure 3 presents SEM-images of various fields of composite fracture PCM-V_4C. Figure 3, *a* shows discernible particles of boron carbide with irregular shape. In Figure 3, *b* you can see distribution of particles inside the composite, and the availability of empty cavities, which are not filled with the particles, since the composite has small filling percentage.

4. Measurement results

4.1. Modelling

Modeling was done for a homogenous mix of composite with the purpose to detect the mechanisms to attenuate the photon radiation, to analyze the contribution of major interactions (photo effect, Compton effect, coherent scattering, pairing) to the full section of interaction of γ-quanta with the material, comparison of photon radiation attenuation in different composites, study of the changes in the nature of interaction of γ-quanta with the substance upon addition of TiH_2 and detection of differences between PCM-V_4C and PCM-V_4C-TiH_2.

Modeling was carried out using software XCOM 3.1 (M.J. Berger, J.H. Hubbell) with the built-in library of partial interaction sections. The data output by the software is

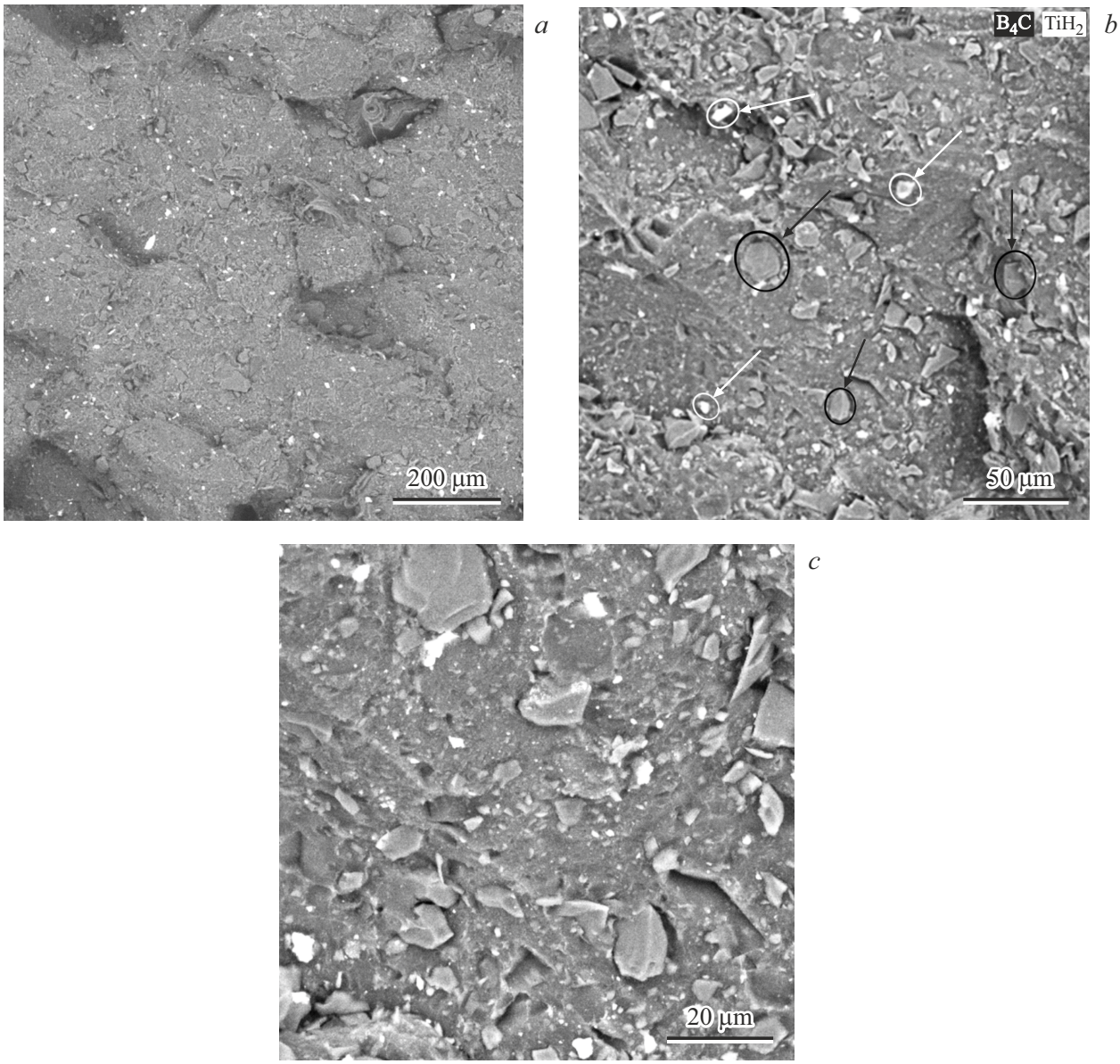

Figure 2. Composite material fracture microphotographs PCM-V_4C-TiH_2.

carried out in full and partial microscopic mass sections of interaction (Σ^m), however, for more convenience further you can see full and partial microscopic sections (σ), the transition to which was done using formula:

$$\mu = \frac{\mu^m}{\rho}, \qquad (1)$$

where μ^m — mass section of material interaction, cm^2/g; ρ — nuclear density of material, nucleus/cm^3. According to the data of modeling results analysis for composite PCM-V_4C Figure 4, *a*, in virtue of high content of light elements (^1H, ^{10}B, ^{12}C), for photons with energy of more than 0.2 MeV the contribution of photo effect practically disappears. In the range of 1−7 MeV the main mechanism of attenuation is the Compton effect, which prevails due to high probability of photon interaction with electrons of light atoms. The contribution of formation of electron-positron pairs starts manifesting itself at energies from 5 MeV, but becomes considerable only at higher energies (above 10 MeV). Analysis of modeling for composite PCM-V_4C-TiH_2 (Figure 4, *b*) showed that addition of TiH_2 changes the nature of interaction of γ-quanta, causing increased contribution of photo effect in the range of 0.1−0.7 MeV, which is related to the presence of titanium having a higher atomic number. Coherent scattering of photons in bonded electrons also increases substantially compared to material PCM-VV_4C, especially in the low energy field. The contribution of formation of electron-positron pairs becomes noticeable already at 5 MeV, which differs this composite from PCM-V_4C, where this effect starts appearing at higher

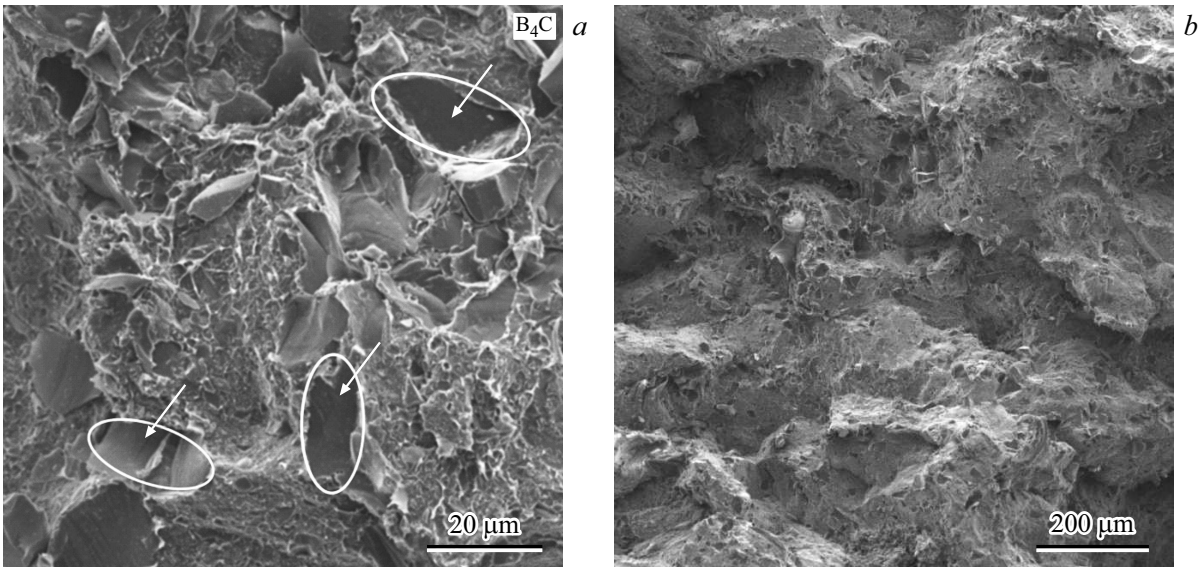

Figure 3. Composite material fracture microphotographs PCM-V_4C.

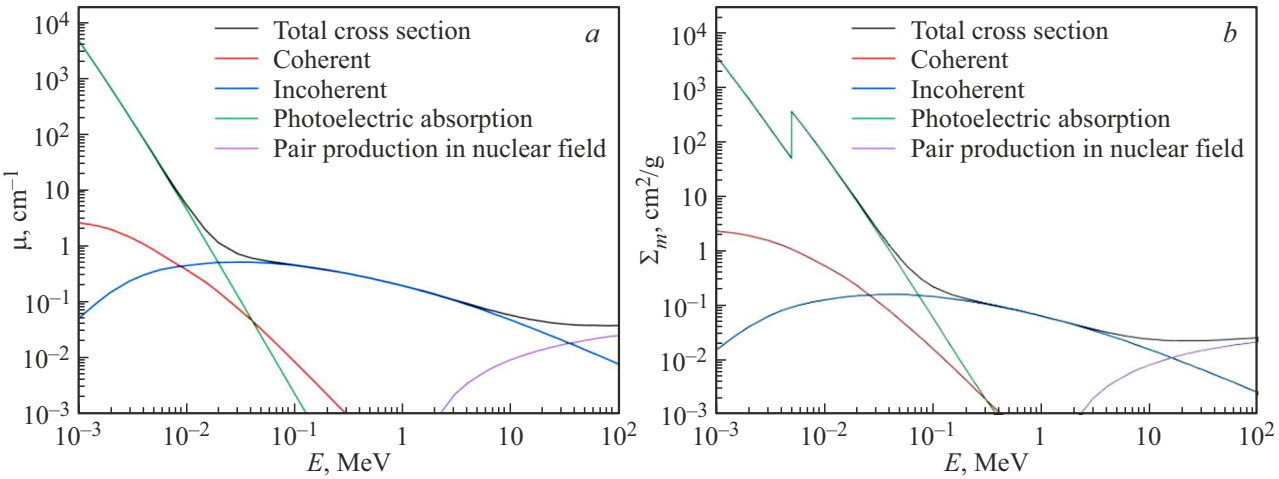

Figure 4. Dependence of full and partial sections of photon radiation interaction with materials of composites PCM-V_4C (*a*) and PCM-V_4C-TiH_2 (*b*).

energies. In the range of 1−7 MeV the Compton effect still prevails, but the interaction section is in general higher than in PCM-V_4C, due to the contribution of other processes.

Therefore, modeling confirms that modification of the material composition makes it possible to control the interaction mechanisms of γ-quanta, optimizing protective properties of composite depending on the range of radiation energy.

4.2. Experimental studies

This paper measured energy spectra of fast neutrons and γ-quanta for composite PCM-V_4C and special composite protective material PCM-V_4C-TiH_2. Measurement results are presented in Figures 5−10.

Figure 5 shows measured energy distributions of γ-quanta flux density, and Figure 6 presents energy distributions of neutron flux density using composite materials as a screening material and without one.

From Figure 5 it follows that both composites substantially decrease the γ-quanta flux in the entire energy range, especially in the area of low energies (< 1 MeV), where photo effect prevails. At energies 1−7 MeV the attenuation is mostly due to Compton effect. In the range above 7 MeV the process of electron-positron pairs formation starts contributing, being especially noticeable at energies above 8 MeV. PCM-V_4C-TiH_2 (dotted line) attenuates the γ-quanta flux more than PCM-V_4C. This is due to the fact that the presence of TiH_2 increases the contribution of photo effect in the area of low energies and formation of electron-positron pairs in the field of high energies.

Coherent scattering also plays a role at low energies, especially for PCM-V_4C-TiH_2. Figure 6 demonstrates that both composites reduce the intensity of neutron flux, especially in the field of low and medium energies (down to 8 MeV). Attenuation of the neutron flux is related to scattering and absorption mechanisms, including elastic and inelastic scattering, and also capturing reactions. The data analysis shows that composite PCM-V_4C-TiH_2 demonstrates more pronounced reduction of neutron flux compared to composite PCM-V_4C. This is related to the presence of titanium hydride (TiH_2), which effectively absorbs and moderates neutrons, increasing the share of elastic scattering in hydrogen nuclei. At energies above 8–10 MeV the differences between composites become less pronounced, since there nuclear reactions of interaction with heavier elements prevail.

To produce the results of full sections, we use the known equation for „unscattered“ component of radiation:

$$F_H(E) = F_0(E)\exp\bigl(-n\sigma(E)x\bigr), \qquad (2)$$

where n — nuclear density of material (nucleus/cm^3), $\sigma(E)$ — target cross section (cm^2), x — specimen thickness (cm).

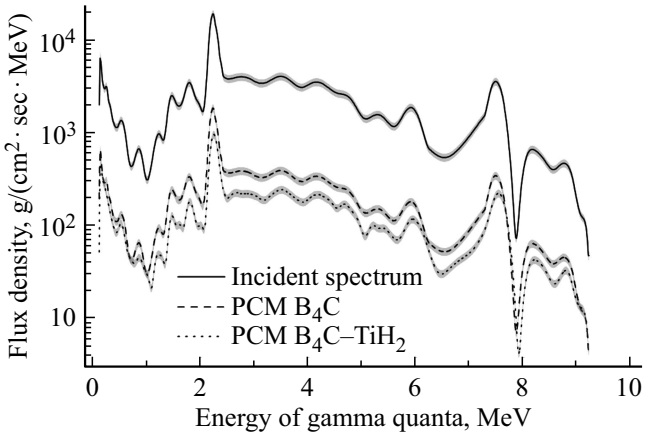

Figure 5. Measured energy distributions of γ-quanta flux density.

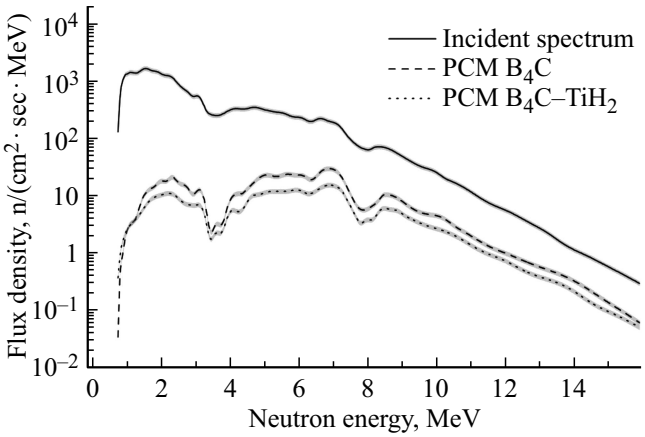

Figure 6. Measured energy distributions of neutron flux density.

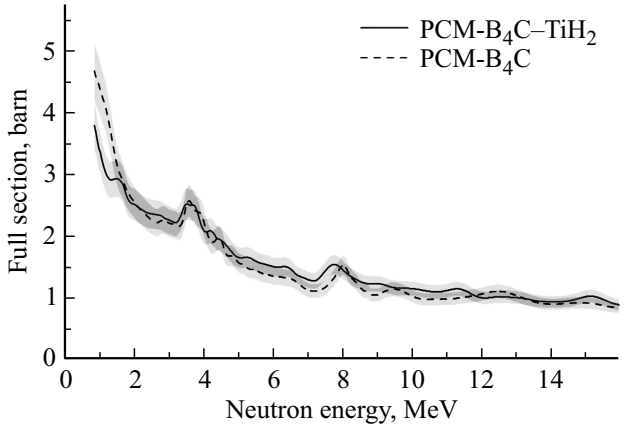

Figure 7. Energy distribution of full neutron section.

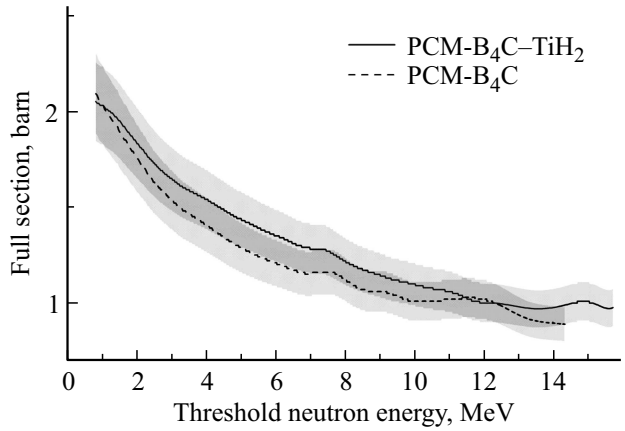

Figure 8. Distributions of full section from threshold energy of neutrons.

Full sections may be calculated using formula (3):

$$\sigma(E) = (1/(nx))\ln\bigl(F_0(E)/F_H(E)\bigr). \qquad (3)$$

Results of calculations of full sections using formula (3) for neutrons are presented in Figures 7 and 8 and for γ-quanta in Figures 9 and 10.

These figures show the dependences of full section of interaction (in barns) on energy of neutrons (MeV) for two composites. The main results may be noted. In Figure 7 in the area of low energies (up to 4 MeV) the interaction section is noticeably higher, which is related to elastic and inelastic scattering of neutrons. As neutron energy increases, the full section gradually decreases, being stabilized in the range of 8–15 MeV. Composite PCM-B_4C-TiH_2 demonstrates slightly larger section, especially in lower energies, which is explained by additional contribution of interaction with hydrogen atoms (from TiH_2). In Figure 8 you can see that in the area of low energies (up to 4–5 MeV), the section is noticeably higher, which is related to processes of neutron moderation and absorption. As the threshold energy increases, the full section decreases, especially after

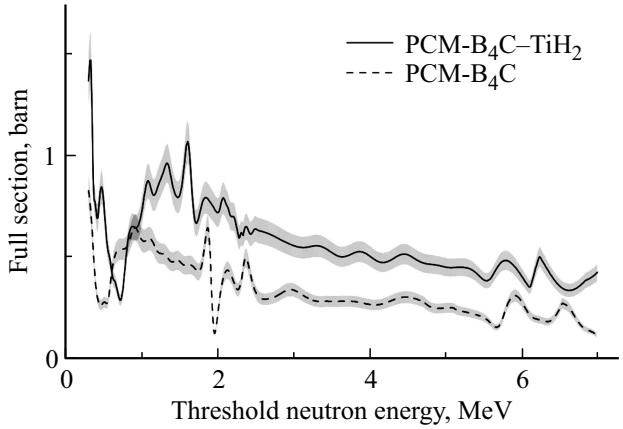

Figure 9. Distribution of energy of full section of γ-quanta.

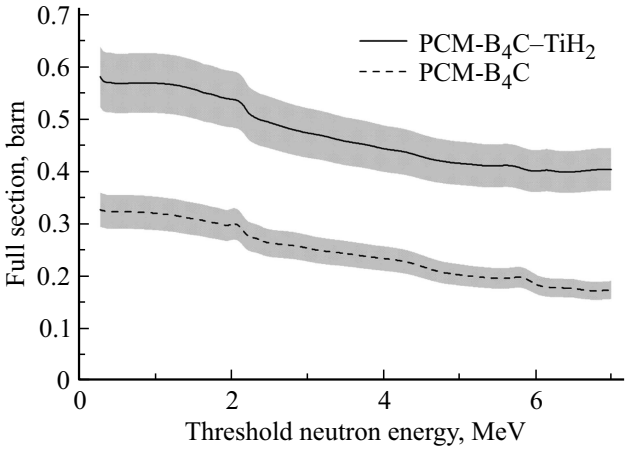

Figure 10. Distributions of full section from threshold energy of γ-quanta.

6–8 MeV, where other scattering mechanisms prevail. As in the first case, PCM-B_4C-TiH_2 demonstrates a slightly larger section, which confirms its higher efficacy in absorption and scattering of neutrons compared to PCM-B_4C. Addition of TiH_2 promotes more effective moderation of neutrons.

Special attention should be paid to data in Figure 9, where the wide area of resonant structures is seen. In this figure the resonant structure manifests itself as oscillations in the range of 0–2 MeV. In the area of $E < 1$ MeV a peak of full section is observed, which is explained by the resonance capture of neutrons in boron carbide (effective section of B-10 neutron absorption) and potential scattering at TiH_2. The difference between PCM-B_4C and PCM-B_4C-TiH_2 is explained by the fact that TiH_2 additionally interacts with the neutrons, creating additional dispersion. As for the resonance structure in the range of 1–3 MeV, in this area one may see well the oscillations of full section, caused by resonance scattering in titanium nuclei. Titanium (especially isotope Ti-48) has several resonance levels of neutron capture in this energy range. Hydrogen in the composition of titanium hydride may transfer some energy to the neutron, modifying its kinematic spectrum. Oscillations in B_4C, related to excited states of nucleus. The difference between curves PCM-B_4C-TiH_2 and PCM-B_4C is especially visible, the solid line with TiH_2 shows a large full section, which means additional absorption of neutrons and scattering at TiH_2. In the area above 3–4 MeV the resonance absorption decreases, and contribution of inelastic scattering becomes dominating. Full section reduces, but oscillations remain subtle, being related to reactions of inelastic scattering in atoms of titanium and nuclear reactions with participation of B_4C, including nucleus splitting. After 6 MeV the difference between PCM-B_4C and PCM-B_4C-TiH_2 decreases, since the effect of neutron moderation becomes less significant. Contributions TiH_2 and B_4C determine a complex pattern of peaks and droops in the section, with a trend towards decrease after 6 MeV. Contribution of TiH_2 is expressed in the decrease of total section in the area of 1–4 MeV, which is explained by scattering and absorption in titanium. Main differences between PCM-B_4C-TiH_2 and PCM-B_4C are due to the presence of titanium and hydrogen, which improve the probability of scattering, increasing the integral section. Upon spectra integration, these oscillations are smoothened, since resonance peaks and inelastic interactions in the energy range are averaged. Error of energy calibration ($\leq 2.5\,\%$) also impacts the precision of section value definition. Upon integration of spectra this problem is naturally resolved (Figure 10).

From the provided results for the full section of neutrons it is clear that material PCM-V_4C-TiH_2 has advantages compared to protective material PCM-B_4C in the energy range from 2 to 10 MeV of around ~ 200 mbarn, at energies from 11.3 to 12.4 MeV there is no difference, however, with further increase of the energy the material PCM-V_4C-TiH_2 has an obvious advantage (due to inelastic scattering of fast neutrons in nuclei of heavy elements).

From the provided results of full section for γ-quanta you can see that material PCM-V_4C-TiH_2 has an obvious advantage to PCM-V_4C (~ 250 mbarn in the entire presented energy range of γ-quanta).

Based on the produced data on energy distributions of neutron (γ-quanta) flux density $F_0(E)$ and energy distributions of neutron (γ-quanta) flux density downstream the studied specimen $F_H(E)$, the attenuation coefficient was calculated using formula (4):

$$K = \frac{F_0(E)}{F_H(E)}. \tag{4}$$

Table 3 presents estimate data on coefficient of neutron flux attenuation by studied materials, and Table 4 — data on coefficient of γ-quanta flux attenuation.

Therefore, addition of TiH_2 to protective material from borated polyethylene in the above quantities increases its protective characteristics for fast neutrons. In the same manner for γ-quanta the addition of a heavy component to borated polyethylene improves protective characteristics of such composite material.

Table 3. Data on coefficient of neutron flux attenuation by studied materials

Material	Coefficient of neutron flux attenuation by studied materials, cm^{-1}							
	Neutron energy E, MeV							
	0.81	1.1	2.0	4.0	7.0	10.0	13.0	16.0
PCM-B_4C	1183.8	428.1	73.3	37.7	6.7	5.6	4.7	4.6
PCM-V_4C-TiH_2	993.8	472.4	128.5	59.9	12.6	9.9	7.3	5.6

Table 4. Data on coefficient of gamma-quanta flux attenuation by studied materials

Material	Coefficient of gamma-quanta attenuation with studied materials, cm^{-1}							
	Energy of gamma-quanta E, MeV							
	0.2	0.6	0.8	1.6	2.5	4.0	6.0	9.0
PCM-B_4C	10.31	11.34	10.32	10.32	10.3	10.35	10.52	11.43
PCM-V_4C-TiH_2	11.37	14.9	14.67	19	19.22	16.9	15.57	12.65

Therefore, it may be concluded that composite material PCM-V_4C-TiH_2 is quite a good compromise between protection against neutrons and protection against γ-radiation, at least in the studied range of radiation energies, and has good physical and technological properties to manufacture reactor protection compositions.

5. Conclusion

The advantage of PCM-B_4C-TiH_2 above PCM-B_4C practically in the entire energy range (except for $E < 1.5$ MeV) is explained by the fact that titanium hydride (TiH_2) contains hydrogen, which more effectively moderates neutrons due to elastic scattering. Despite the fact that titanium itself plays a role in inelastic scattering, the main role in neutron energy reduction is played by hydrogen in TiH_2, and not titanium itself. At $E < 1.5$ MeV the advantage stays with B_4C, since boron has very high section of thermal neutron absorption.

Therefore, addition of heavy material to borated polyethylene in the above quantities does not deteriorate its protective characteristics for neutrons, and with titanium hydride it even somewhat improves them. For γ-quanta the addition of a heavy material to borated polyethylene naturally improves protective characteristics of such composite material.

It should also be noted that composite material PCM-V_4C-TiH_2 is quite a good compromise between protection against neutrons and protection against gamma-radiation, at least in the studied range of radiation energies, and has good physical and technological properties to manufacture protection compositions.

Acknowledgments

The study was performed using equipment on the base of the High Technology Center of V.G. Shukhov Belgorod State Technology University.

Conflict of interest

The authors declare that they have no conflict of interest.

References

[1] R. Apkin. Procedia — Soc. Behav. Sci. **149**, 59–64 (2014).
[2] C. Guo, Q. Wang, P. Shuai, T. Wang, W. Wu, Y. Li, S. Huang, J. Yu, L. Yi. Chemosphere **357**, 142030 (2024).
[3] J.J. Broerse. in Advances in Radiation Protection and Dosimetry in Medicine / Editors: R.H. Thomas, V. Perez-Mendez. Springer, US (1980) p. 415–429.
[4] R.N. Ihsani, P.L. Gareso, D. Tahir. Radiat. Phys. Chem. **218**, 111619 (2024).
[5] M. Asgari, H. Afarideh, H. Ghafoorifard, E.A. Amirabadi. Nucl. Eng. Technol. **53**, *12*, 4142–4149 (2021).
[6] F. Erdogan, B. Goddard, R. Mohammadi, J.V. Rojas. Radiat. Phys. Chem. **222**, 111884 (2024).
[7] W. Abdullah, R.M. Ramli, T.H. Khazaalah, N.Z.N. Azman, T.M. Nawafleh, F. Salem. Nucl. Eng. Technol. **56**, *9*, 3608–3615 (2024).
[8] Muh. Ilham Akbar, B. Armynah, D. Tahir. Ind. Crops Prod. **222**, 119440 (2024).
[9] S.M. Kassem, S.R. El-Shawadfy, N.A. Kotb. Prog. Nucl. Energy. **176**, 105393 (2024).
[10] H. He, Y. Xu, B. Zhang, Q. Wang, W. Li, Y. Cai. J. Energy Storage **100**, 113465 (2024).
[11] A.M. El-Khatib, M.T. Alabsy, A.Y. El-Khatib, M.F. Dib, M.I. Abbas. Nucl. Eng. Technol. **56**, *10*, 4103–4114 (2024).
[12] M. Yílmaz, F. Akman. Appl. Radiat. Isot. **200**, 110994 (2023).
[13] J.C. Knott. Compos. Sci. Technol. **233**, 109876 (2023).
[14] F. Erdogan, B. Goddard, R. Mohammadi, J.V. Rojas. Radiat. Phys. Chem. **222**, 111884 (2024).
[15] N.I. Cherkashina, V.I. Pavlenko, A.N. Shkaplerov, A.A. Kuritsyn, R.V. Sidelnikov, E.V. Popova, L.A. Umnova, S.N. Domarev. Adv. Space Res. **73**, *5*, 2638–2651 (2024).
[16] H. Ogul, B. Gultekin, H. Yildiz, H. Us, F. Bulut. Radiat. Phys. Chem. **219**, 111686 (2024).
[17] G. Almisned, G. Susoy, H.O. Tekin. Radiat. Phys. Chem. **218**, 111585 (2024).

[18] J. Rataj, P. Suk, T. Bílý, M. Štefánik, J. Frýbort. Appl. Radiat. Isot. **168**, 109529 (2021).
[19] C. Kursun, M. Gao, A.O. Yalcin, K.A. Parrey, Y. Gaylan. Ceram. Int. **50**, *15*, 27154–27164 (2024).
[20] X. Huang, Z. Du, Y. Li, Z. Li, X. Yang, M.-J. Li. Energy **302**, 131813 (2024).
[21] M.A. Al Zaman, N.J. Monira. Radiat. Phys. Chem. **205**, 110706 (2023).
[22] M. Naito, S. Kodaira, R. Ogawara, K. Tobita, Y. Someya, T. Kusumoto, H. Kusano, H. Kitamura, M. Koike, Y. Uchihori, M. Yamanaka, R. Mikoshiba, T. Endo, N. Kiyono, Y. Hagiwara, H. Kodama, S. Matsuo, Y. Takami, T. Sato, S. Orimo. Life Sci. Space Res. **26**, 69–76 (2020).
[23] H.-W. Li, Y. Yan, S. Orimo, A. Züttel, C.M. Jensen. Energies **4**, *1*, 185–214 (2011).
[24] P. Rudnev, I. Cheshigin. Elektronika, nauka, tekhnologiya, biznes **4**, 00225 (2023). (in Russian).

Translated by M.Verenikina